AIAA JOURNAL
Vol. 44, No. 11, November 2006

Direct Numerical and Large-Eddy Simulations of Turbulent Flows over Rough Surfaces

Stefano Leonardi*
University of Rome "La Sapienza," 00184 Rome, Italy
Fabrizio Tessicini†
Imperial College London, London, England SW7 2AZ, United Kingdom
Paolo Orlandi‡
University of Rome "La Sapienza," 00184 Rome, Italy
and
Robert Antonia§
University of Newcastle, Newcastle, New South Wales 2308, Australia

Direct numerical simulations (DNS) and large-eddy simulations (LES) of a turbulent channel flow with transverse square bars on one wall have been carried out at $Re = 6.9 \times 10^3$. Both the Smagorinsky, with Van Driest damping, and dynamic subgrid models have been used. There is satisfactory agreement between the two types of simulations for the pressure and skin friction on the wall and the rms velocity near the wall. Far from the wall, LES gives only an approximation of the rms distributions obtained by DNS. However, the subgrid models are a significant improvement relative to when no model is used (which corresponds to an unresolved DNS). Another DNS at $Re = 1.2 \times 10^4$ has been performed with the aim of comparing the results with the experiment by (Hanjalic, K., and Launder, B. E., "Fully Developed Asymmetric Flow in Plane Channel," *Journal of Fluid Mechanics*, Vol. 51, 1972, pp. 301–335). The agreement between mean and rms distribution is good. The Reynolds-number dependence (Re ranging from 2.8×10^3 to 1.2×10^4) has been discussed. The pressure on the wall and hence the form drag do not depend on Reynolds number, and the velocity profile changes slightly for $Re > 6.9 \times 10^3$.

Nomenclature

C_f = skin-friction coefficient
d = error in origin
h = half-width of the channel
k = roughness height
$\boldsymbol{n}$ = unit vector normal to the wall
P = pressure
p = longitudinal separation between consecutive bars
Re = $U_b h/\nu$, Reynolds number
$\boldsymbol{s}$ = unit vector tangent to the wall
U_b = bulk velocity
U_c = centerline velocity
U_i = component of the velocity vector in the i direction
U_τ = friction velocity
u = streamwise velocity fluctuation
v = wall-normal velocity fluctuation
w = spanwise velocity fluctuation
x = streamwise direction
$\boldsymbol{x}$ = unit vector along x
y = wall-normal direction (origin at the centerline)
$\tilde{y}$ = wall-normal direction (origin on the bottom wall)
z = spanwise direction
ΔU^+ = roughness function
λ = streamwise wavelength
ν = kinematic viscosity
Π = pressure gradient required to maintain a constant flow rate
τ_w = wall shear
$\langle\,\rangle$ = averaging with respect to time and z

Subscripts

$+$ = normalization by either U_τ or ν/U_τ
$-$ = averaging with respect to time x and z

Presented as Paper 2005-4808 at the AIAA 4th Theoretical Fluid Mechanics Meeting, Toronto, ON, Canada, 6–9 June 2005; received 2 September 2005; revision received 19 January 2006; accepted for publication 21 January 2006.

*Research Associate, Dipartimento di Meccanica ed Aeronautica; currently Assistant Professor, Department of Mechanical Engineering, University of Puerto Rico, Mayaguez, PR 00681-9045.
†Research Associate, Department of Aeronautics.
‡Full Professor, Dipartimento di Meccanica ed Aeronautica.
§Full Professor, Discipline of Mechanical Engineering.

Introduction

FLOWS over rough surfaces are of interest in many practical applications, ranging from shipbuilding and aviation, the flows over blades in different types of turbomachines, and the flows over vegetated surfaces in the atmospheric surface layer. In an engineering context, pipes and ducts cannot be regarded as hydraulically smooth, especially at high Reynolds numbers. Rough surfaces can be used to enhance heat transfer as in computer processors coolers. The roughness geometry can be selected so as to decrease the drag, for example, by using riblets or delaying transition. Artery walls can be rough as a result of the stenosis built up by the cholesterol.

Despite the practical importance of the flow, the knowledge of turbulent rough wall flows is far from complete. According to the classical scheme (e.g., Clauser,[1] Perry et al.,[2] and Raupach et al.[3]), the rough wall boundary condition affects the mean velocity distribution in the inner region (in the case of a channel flow, $y/h < 0.2$). The effect of the roughness is to shift the mean velocity profile, with respect to that on a smooth wall, by an increment ΔU^+, referred to as the roughness function. The roughness function depends on the density (defined as the total roughness frontal area per unit wall area), height k, and nature of the roughness. Orlandi et al.[4] showed that ΔU^+ is very well correlated with the rms of the wall-normal velocity.

The effect of the roughness on the outer layer remains a somewhat controversial issue. This is mostly because of general difficulties in making reliable measurements in the vicinity of the roughness elements. The wall shear stress is usually inferred by

the Clauser method. However, Perry and Joubert[5] outlined that several combinations of U_τ, ΔU^+, and error in origin can be found for the same velocity profile. Direct numerical simulations can provide an accurate determination of the wall shear τ_w at least when Reynolds number is small. They also allow quantification of the relative contributions to τ_w of the form and skin-frictional drag. Leonardi et al.[6] showed the distributions of $\langle C_f \rangle$ and $\langle P \rangle$ for a range of p/k [where p is the streamwise separation between consecutive bars, $\langle C_f \rangle = 1/Re\,\partial\langle U \rangle/\partial y$ on the wall, $Re = U_b h/\nu < 10^3$, U is scaled with U_b and y with h, $\langle P \rangle$ is the pressure, and angular brackets denote averaging with respect to time and z]. For $w/k > 7$, the roughness elements are isolated because the strength and size of the main recirculation zone no longer depend on p/k. The minimum $\overline{C_f}$ and maximum $\overline{P_d}$ occur at $p/k = 7$ when the reattachment on the bottom wall occurs immediately upstream of the subsequent element

$$\overline{P_d} = \lambda^{-1} \int_0^\lambda \langle P \rangle \boldsymbol{n} \cdot \boldsymbol{x}\, \mathrm{d}s, \qquad \overline{C_f} = \lambda^{-1} \int_0^\lambda \langle C_f \rangle \boldsymbol{s} \cdot \boldsymbol{x}\, \mathrm{d}s$$

and $\lambda = p + k$ is the streamwise wavelength. For $p/k \leq 2$, the total drag is closely approximated by the skin-frictional drag on the crests of the elements. In the range $5 < p/k < 19$, the total drag is contributed almost entirely by $\overline{P_d}$. One would therefore expect that, for this range, the Reynolds-number dependence would be much smaller than in the former case.

However, in real rough wall flows the Reynolds number is high, and the size of roughness is very small relative to the characteristic length of the outer flow. Jiménez[7] claimed that numerical or laboratory experiments should have at least $\delta/k > 50$ and $k^+ = kU_\tau/\nu$ in the fully rough regime (δ represents either the diameter of the pipe, the thickness of the boundary layer, or the half-width of a duct, and k^+ is the height of the roughness elements in wall units). Because the mesh size needs to be small with respect to k and the computational box much larger than k, numerical simulations require a large number of points even when nonuniform grids are adopted. For this reason, to date, numerical simulations have been carried out only at moderate values of δ/k (usually of the order 10) and at low Reynolds numbers ($Re < 10^3$), for example, direct numerical simulations (DNS) by Miyake, et al.[8] Leonardi et al.,[6] Ashrafian and Anderson,[9] and large-eddy simulations (LES) by Cui et al.[10] Although these simulations have provided useful results, the Reynolds-number dependence has to be addressed if the results are to be of relevance to practical situations. The Reynolds number can be increased with LES. In this context, DNS can be used to test how classical subgrid models perform in turbulent rough wall flows. In the present paper, LES and DNS results of a turbulent channel flow at $Re = 6.9 \times 10^3$ with transverse square bars on the bottom wall with $\lambda/k = 10$ and a smooth upper wall are compared. DNS have been carried out also at $Re = 2.8 \times 10^3$ and $Re = 1.2 \times 10^4$ to address the Reynolds-number dependence and to compare the results with the experiment by Hanjalic and Launder.[11] The computational box is $6.25h \times 2.125h \times \pi h$ in the streamwise x, wall-normal y, and spanwise z, direction, respectively. The additional $0.125h$ increase in the channel height is caused by the cavity height where the square elements ($k = 0.125h$) are placed ($-1.125 \leq y/h \leq -1$).

The grid used for the LES ($240 \times 160 \times 49$ in x, y, z, respectively) is much coarser than that used for the DNS ($512 \times 161 \times 193$ for $Re = 6.9 \times 10^3$ and $1153 \times 161 \times 193$ for $Re = 1.2 \times 10^4$). Ikeda and Durbin[12] carried out a grid-dependence study for the same flow as considered here. At $Re = 6520$, they found similar results for the $1024 \times 352 \times 192$ and $576 \times 352 \times 192$ grids. It would appear that the results are very sensitive to the number of points in z, which, at this Reynolds number, should not be less than 192. The models used for the LES are the standard Smagorinsky model with Van Driest damping ($C_s = 0.1$, hereafter SM10) and the dynamic model (DYN). To underline the effect of the subgrid model, a simulation without model has been carried out (NOM). The latter would correspond to an unresolved DNS.

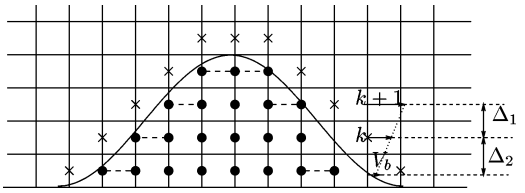

Fig. 1 Geometrical sketch of immersed boundary method: ●, points inside the roughness element and ×, points nearest to the boundary of the roughness element. A partial wavy wall (——) is shown.

Numerical Procedure

The nondimensional Navier–Stokes and continuity equations for incompressible flows are

$$\frac{\partial U_i}{\partial t} + \frac{\partial U_i U_j}{\partial x_j} = -\frac{\partial P}{\partial x_i} + \frac{1}{Re}\frac{\partial^2 U_i}{\partial x_j^2} + \Pi, \qquad \nabla \cdot U = 0 \quad (1)$$

The Navier–Stokes equations have been discretized in an orthogonal coordinate system using the staggered central second-order finite difference approximation. Here, only the main features are recalled because details of the numerical method can be found in Orlandi.[13] The discretized system is advanced in time using a fractional-step method with viscous terms treated implicitly and convective terms explicitly. The large sparse matrix resulting from the implicit terms is inverted by an approximate factorization technique. At each time step, the momentum equations are advanced with the pressure at the previous step, yielding an intermediate nonsolenoidal velocity field. A scalar quantity Φ projects the nonsolenoidal field onto a solenoidal one. A hybrid low-storage third-order Runge–Kutta scheme is used to advance the equations in time. The roughness is treated by the efficient immersed boundary technique described in detail by Fadlun et al.[14] This approach allows the solution of flows over complex geometries without the need of computationally intensive body-fitted grids. It consists of imposing $U_i = 0$ on the body surface which does not necessarily coincide with the grid. Another condition is required to avoid that the geometry is described in a stepwise way. Fadlun et al.[14] showed that second-order accuracy is achieved by evaluating the velocities at the closest point to the boundary using a linear interpolation. This method, which requires a fine grid as the basis of DNS, has been applied to a large number of flows, as described in the review of Iaccarino and Verzicco.[15] As in Fadlun et al.,[14] $U_i = 0$ is imposed in the grid points within the roughness elements. The method here used differs in the treatment of the first point outside the body. The viscous terms are discretized taking into account the real distance between the grid point and the boundary of the roughness elements and not the grid spacing (Fig. 1), that is, for a generic direction,

$$\frac{\partial^2 U}{\partial x^2} = U|_{i+1}\frac{2}{\Delta_1(\Delta_1 + \Delta_2)} - 2U|_i\frac{2}{\Delta_1\Delta_2} \quad (2)$$

$$+U|_{i-1}\frac{2}{\Delta_2(\Delta_1 + \Delta_2)} \quad (3)$$

Results and Discussion

The square element on the bottom wall induces a separation at the trailing edge of the elements ($x/k \simeq 1$; Fig. 2). The flow at $Re = 6.9 \times 10^3$ reattaches on the bottom wall at about $x_R = x/k \simeq 4.56$ (where $x_R = 0$ is taken at the trailing edge of the element). The reattachment length agrees well with the DNS at $Re = 6.520 \times 10^3$ of Ikeda and Durbin,[12] who found $x_R = 4.46$. On the other hand, LES simulations predict a larger recirculating region, with a smaller intensity. As the next element is approached, a separation occurs at about $x/k \simeq 9$, one roughness height upstream of the element. The LES, in this case, yield a good approximation for the C_f with respect to the DNS. This behavior is caused by the nonuniform grid used for the LES with a larger number of points very near the element and a very coarse resolution within

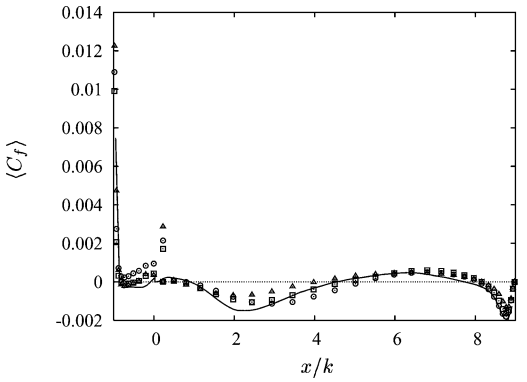

Fig. 2 Normalized skin-friction coefficient on the horizontal walls for one roughness wavelength at $Re = 6.9 \times 10^3$: ——, DNS; △, NOM; ○, Smagorinsky; and □, dynamic.

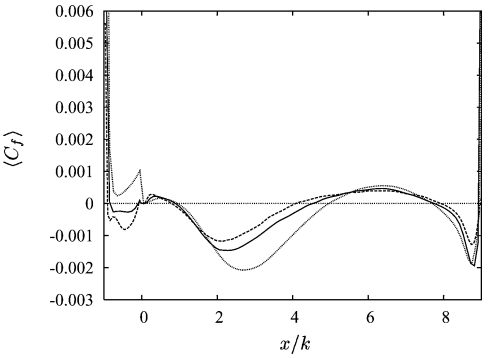

Fig. 3 Normalized skin-friction coefficient on the horizontal walls for one roughness wavelength. DNS results: · · · ·, $Re = 2.8 \times 10^3$; ——, $Re = 6.9 \times 10^3$; and - - - -, $Re = 1.2 \times 10^4$.

the cavity. The element leads to a large increase of velocity and a presence of the friction peak at the leading edge of the element. Above the crest ($0 < p/k < 1$) a separation occurs. Because of the coarse resolution in y and z on the crests plane, LES and NOM do not reproduce this separation, which was also observed in the experiment of Liu et al.[16] This means that a large number of grid points are necessary to resolve the flow scales near the roughness elements. Roughness elements are, therefore, a limitation for the LES simulations because the number of grid points cannot be decreased too much. The Reynolds dependence is addressed through three DNS at $Re = 2.8 \times 10^3$, 6.9×10^3 and 1.2×10^4 (Fig. 3). As the Reynolds number is increased, the reattachment on the bottom wall (first zero crossing) moves toward the trailing edge, and the recirculation region becomes smaller and less intense. On the roughness crest plane at higher Reynolds number, the separation (negative friction) is more intense. Cui et al.[10] carried out an LES at $Re = 10^3$ for $k/h = 0.2$. The reattachment length ($x_R = 4.4$) agrees well with the present DNS results. They also observed a separated flow over the crests plane.

Pressure distributions along the horizontal and vertical walls are shown in Fig. 4 over one wavelength. Very near the element ($0 < x/k < 2$ and $10 < x/k < 12$) LES and DNS results are in good agreement, whereas NOM is a poor approximation. At the center of the cavity, larger differences are found because of the coarser mesh.

The dependence of the pressure on the Reynolds number (Fig. 5) is weaker than that for the frictional drag; the distributions for $Re = 2.8 \times 10^3$, 6.9×10^3 and 1.2×10^4 almost overlap. Because the difference between pressure distributions on the vertical walls corresponds to the form drag for this roughness element, approximately, the LES and DNS yield values of the form drag that agree. On the other hand, NOM yields a different pressure distribution over most of the wavelength and a different (smaller) form drag.

The viscous and form drag are determined by integrating the friction and pressure distribution over one wavelength. By increasing

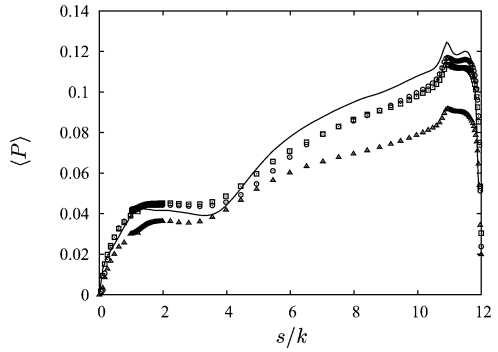

Fig. 4 Pressure along the walls of a roughness wavelength (the coordinate s follows the walls of the cavity; the origin is at the leading edge) for $Re = 6.9 \times 10^3$: ——, DNS; △, NOM; ○, Smagorinsky; and □, dynamic.

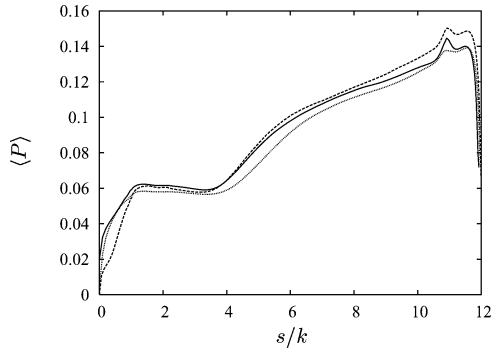

Fig. 5 Pressure along the walls for one roughness wavelength. (The coordinate s follows the walls of the cavity; the origin is at the leading edge.) Legend as in Fig. 3.

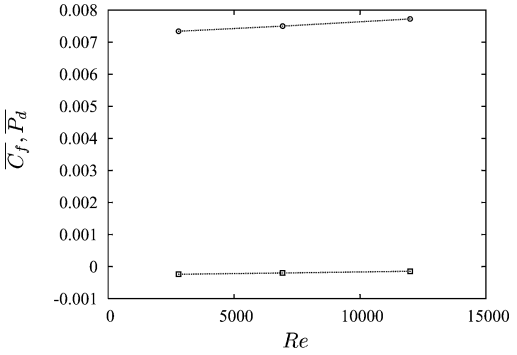

Fig. 6 Dependence of frictional and form drag on the Reynolds number: □, frictional drag and ○, form drag.

the Reynolds number, the form drag does not vary much. It differs by about 5% between $Re = 2.8 \times 10^3$ and $Re = 1.2 \times 10^4$ (Fig. 6). This is an extension of the results of Leonardi et al.[6] In the latter paper, $C_d = \overline{P_d}/k$ was found not to depend on Re (which was varied between $Re = 2.8 \times 10^3$ to $Re = 6.9 \times 10^3$) and on k (in the range $0.1h$ to $0.2h$). For large values of p/k (e.g., $p/k > 3$), the total drag is almost entirely caused by the form drag.[6] Therefore, the value of the friction velocity, $U_\tau \equiv (\overline{P_d} + \overline{C_f})^{1/2}$, does not change with the Reynolds number:

$$\left(\overline{C_f} = \lambda^{-1} \int_0^\lambda \langle C_f \rangle \, \mathrm{d}s \right)$$

As a consequence, we believe that, for this type of roughness, the flow physics near the wall can be investigated through numerical simulations at moderate Reynolds numbers.

The mean velocity distributions, shown in Fig. 7 for different Reynolds numbers, are compared with the measurements of Hanjalic and Launder[11] at $Re = 1.2 \times 10^4$. The agreement between

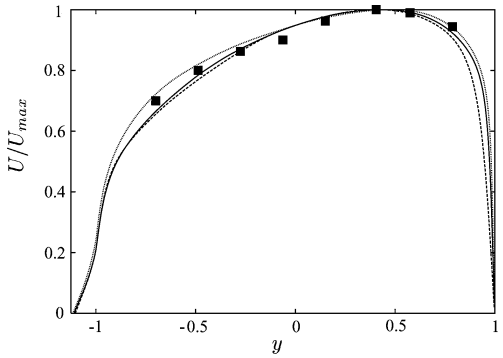

Fig. 7 Mean velocity distribution: symbols, experiment by Hanjalic and Launder[11] lines, DNS; · · · ·, $Re = 2.8 \times 10^3$; ——, 6.9×10^3; and - - - -, 1.2×10^4.

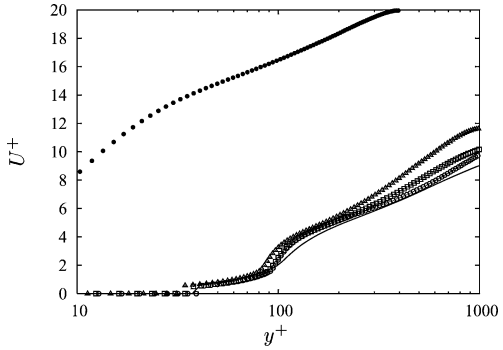

Fig. 8 Mean velocity distribution in wall units: closed symbols smooth wall channel[18]; ——, DNS; △, NOM; ○, Smagorinsky; and □, dynamic at $Re = 6.9 \times 10^3$.

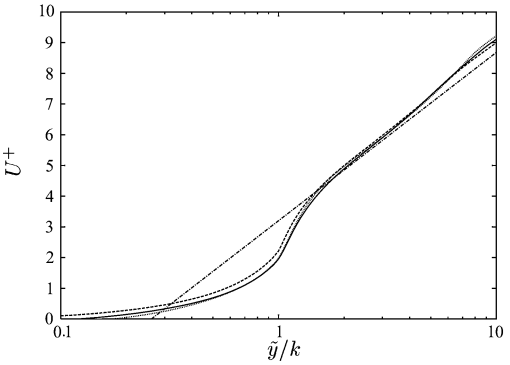

Fig. 9 Mean velocity distribution in wall units. The straight line (—·—) is an empirical equation proposed by Hanjalic and Launder,[11] $[U^+ = 1/0.42\ell_n y/k) + 3.2]$. Lines present DNS: · · · ·, 2.8×10^3; ——, 6.9×10^3; and - - - -, 1.2×10^4.

experiment and DNS is satisfactory. The DNS results show that by increasing Reynolds number the maximum velocity is shifted upward (toward the smooth wall). This is because of the increased value of the ratio between the rough wall and smooth wall friction velocities.[17] However, whereas the changes to the velocity profile are large between $Re = 2.8 \times 10^3$ and 6.9×10^3, only slight differences are observed between $Re = 6.9 \times 10^3$ and 1.2×10^4. Therefore, the dependence on the Reynolds number, for intermediate values of Re is weak even in the outer layer, so that DNS is a useful tool for providing insight into rough flows.

The velocity profile in wall units is

$$U^+ = \kappa^{-1}\,\ell_n\ y^+ + C - \Delta U^+ \tag{4}$$

where C and κ are constants and $+$ denotes normalization by either U_τ or ν/U_τ. The origin for y, (d/k), is inferred by fitting the mean velocity data to Eq. (4) after assuming $\kappa = 0.41$. With respect to the smooth wall, the velocity profile is shifted downward by a factor ΔU^+, known as the roughness function. In Fig. 8, the mean velocity profiles in wall units for DNS, LES, and NOM are compared to the smooth wall distribution by Moser et al.[18] As expected, the mean velocity profile is shifted downward, and the agreement between LES and DNS is reasonable. The roughness function is indeed caused essentially by the increase of U_τ. For this value of λ/k, U_τ is mostly caused by the pressure distribution, which was shown to be similar for DNS and LES (Fig. 4). On the other hand, the pressure drag for NOM was different from that relative to the DNS, and then larger differences to the velocity profile are expected. Even if U_τ does not change, the roughness function increases by increasing the Reynolds number. In fact, because k, U_τ, and the error in origin do not vary, increasing the Reynolds number leads to an increase of k^+. Perry et al.[2] showed that, for large λ/k (k-type roughness),

$$\Delta U^+ = \kappa^{-1}\,\ell_n\,k^+ + B \tag{5}$$

The value of k^+ is 80, 103, and 180 for $Re = 2.8 \times 10^3$, 6.9×10^3, and 1.2×10^4, respectively. The corresponding values of ΔU^+ are 12.9, 13.5, and 14.8, respectively, in agreement with Eq. (5), with $B = 2.6$ and $C = 5.5$. Cui et al.[10] at $Re = 10^3$, by an LES for the same λ/k but larger roughness elements $(k/h = 0.2)$, found $k^+ = 320$ and $\Delta U^+ = 16$. It agrees reasonably with the present results and Eq. (5), with $B = 2.1$ and $C = 5.5$. These values of k^+ correspond

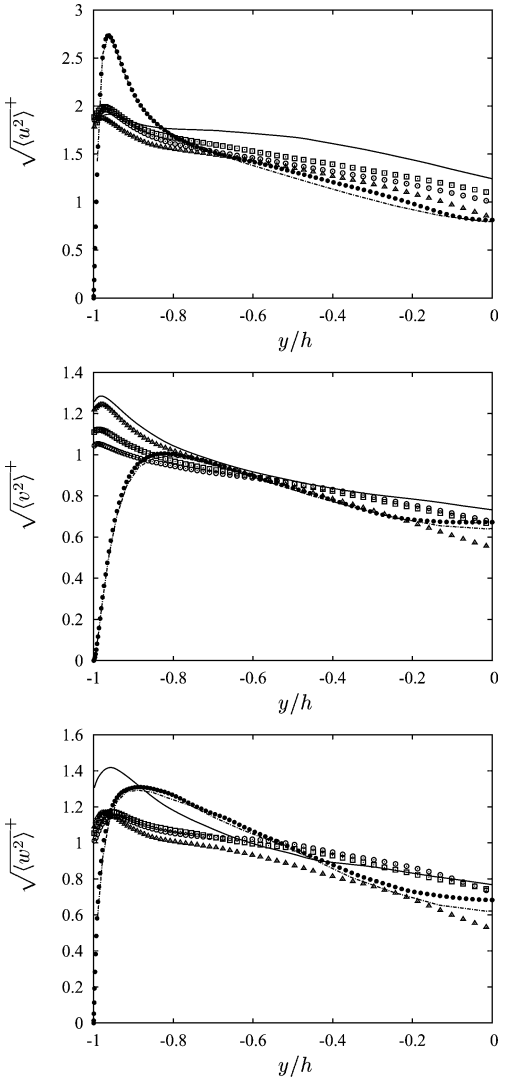

Fig. 10 Normal turbulent intensities scaled in wall units, $Re = 6.9 \times 10^3$: ——, DNS; △, NOM; ○, Smagorinsky; and □, dynamic. The smooth wall channel distributions are included as reference: ●, Moser et al.[18]; and —·—, DNS.

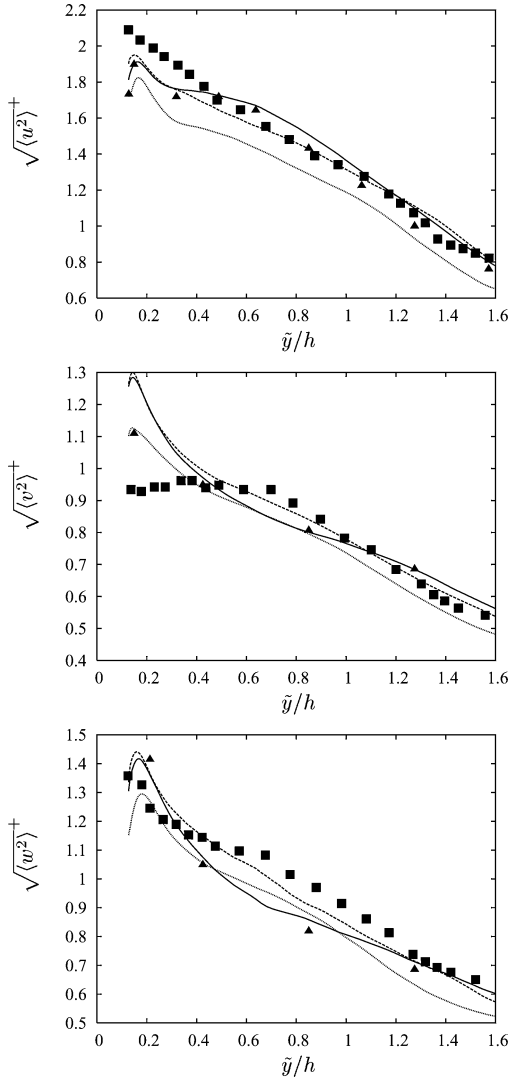

Fig. 11 Turbulent intensities in wall units: ····, $Re = 2.8 \times 10^3$; ——, $Re = 6.9 \times 10^3$; - - - -, $Re = 1.2 \times 10^4$; ■, Hanjalic and Launder[11] at $Re = 1.8 \times 10^4$; and ▲, Ikeda and Durbin[12] at $Re = 6520$.

to the fully rough regime.[19] Hanjalic and Launder[11] found that, for several values of Re (1.8×10^4 to 5.5×10^4), U^+, in the log region, agrees well with the empirical equation $U^+ = 1/0.42\,\ell_n(y/k) + 3.2$. Present DNS results, and the DNS results by Ikeda and Durbin[12] (not shown here), even at lower Reynolds numbers (from 2.8×10^3 to 1.2×10^4) agree well with the results of Hanjalic and Launder[11] (Fig. 9). Therefore, for a wide range of Reynolds U^+ is constant at a given $\tilde{y}/k$ ($\tilde{y}$ has the origin on the bottom wall). This means that the increase of the roughness function is caused by the error in origin. Even if by increasing the Reynolds number d/k is constant, d^+ increases. To a larger d^+ corresponds a larger sideway shift of the velocity profile and then a larger roughness function.

Turbulent intensities scaled in wall units are shown in Fig. 10. Near the wall ($y/h = -1$), for $\sqrt{\langle u^2\rangle}^+$, both the large-eddy simulations performed with Smagorinsky and dynamic models agree reasonably well with the DNS. The other two stresses are only an approximation of the DNS result, especially $\sqrt{\langle w^2\rangle}^+$. Larger difference for $\sqrt{\langle v^2\rangle}^+$ and $\sqrt{\langle u^2\rangle}^+$ can be discerned in the inner part of the channel. The improvement brought about by the subgrid models that have been tried is encouraging. Indeed, with respect to NOM, LES compare much better with the DNS results. Despite an increase in $\sqrt{\langle u^2\rangle}$ (not shown here), $\sqrt{\langle u^2\rangle}^+$ is largely reduced consistently with the DNS by Bhaganagar et al.,[20] of a turbulent channel flow with three-dimensional roughness on one wall. As expected, near the roughness crests plane ($y/h = -1$) $\sqrt{\langle v^2\rangle}^+$ and $\sqrt{\langle w^2\rangle}^+$ are larger than over a smooth wall. The normal wall velocity is the quantity most affected by the rough wall. Orlandi et al.[21] showed that the salient characteristic of rough wall flows is the presence of a nonzero wall-normal normal velocity distribution at the interface between the roughness cavities and the external flow. Near a rough wall, $\sqrt{\langle v^2\rangle}^+$ and $\sqrt{\langle w^2\rangle}^+$ increase, whereas $\sqrt{\langle u^2\rangle}^+$ is reduced; therefore, isotropy is better approximated than over a smooth wall in agreement with Smalley et al.[22] and Krogstad et al.[23] Far from the wall, at about $10k$, the turbulent intensities relative to a rough wall differ from those of a smooth wall channel. Orlandi and Leonardi[24] showed that as y is scaled with the distance between the rough wall and the zero crossing of $\overline{uv}$ the rms distributions, relative to four different rough surfaces, far from the wall almost overlap. Larger values of h/k have to be investigated in order to assess properly Townsend's similarity hypothesis.[7]

The dependence of the turbulent intensities on the Reynolds number is shown in Fig. 11. Regardless of the differences in k^+ and ΔU^+, turbulent intensities agree closely throughout the channel. Hanjalic and Launder[11] performed an experiment at higher Reynolds numbers in a channel with square bar roughness. In agreement with the present results, they found that the turbulent intensities, scaled in wall units, do not depend on the Reynolds number.

Experimental data and DNS distributions of $\sqrt{\langle u^2\rangle}^+$ and $\sqrt{\langle w^2\rangle}^+$ agree well, whereas slight differences near the wall (about 20%) are found for $\sqrt{\langle v^2\rangle}^+$. This can be because of experimental difficulties in measuring the wall-normal velocity fluctuations near the roughness crests. In the outer region DNS results and experimental data compare well.

Conclusions

Direct and large-eddy simulations have been performed for a turbulent channel flow with transverse square bars on the bottom wall with a pitch to height ratio λ/k of 10 at $Re = 2.8 \times 10^3$, 6.9×10^3, and 1.2×10^4. For both form and frictional drag the agreement between DNS and LES is satisfactory. Near the wall, the rms velocity obtained with LES compares reasonably well with DNS results. Far from the wall larger differences are found. However, the improvement associated with the subgrid model with respect to an unresolved DNS is encouraging. The DNS at $Re = 1.2 \times 10^4$ is in reasonable agreement with the experiment of Hanjalic and Launder.[11] The Reynolds-number dependence for intermediate Re is quite weak, especially for pressure drag and rms velocity. Therefore we believe that DNS and LES can be very useful for studying of rough wall flows at least for high values of λ/k.

References

[1]Clauser, F. H., "Turbulent Boundary Layers in Adverse Pressure Gradients," *Journal of the Aeronautical Sciences*, Vol. 21, 1954, pp. 91–109.

[2]Perry, A. E., Schofield, W. H., and Joubert, P. N., "Rough Wall Turbulent Boundary Layers," *Journal of Fluid Mechanics*, Vol. 37, 1969, pp. 383–413.

[3]Raupach, M. R., Antonia R. A., and Rajagopalan, S., "Rough-Wall Turbulent Boundary Layers," *Applied Mechanics Reviews*, Vol. 44, 1991, pp. 1–25.

[4]Orlandi, P., Leonardi, S., and Antonia, R. A., "Turbulent Channel Flow with Either Transverse or Longitudinal Roughness Elements on One Wall," *Journal of Fluid Mechanics*, Vol. 561, 2006, pp. 279–305.

[5]Perry, A. E., and Joubert, P. N., "Rough Wall Boundary Layers in Adverse Pressure Gradients," *Journal of Fluid Mechanics*, Vol. 17, 1963, pp. 193–211.

[6]Leonardi, S., Orlandi, P., Smalley, R. J., Djenidi, L., and Antonia, R. A., "Direct Numerical Simulations of Turbulent Channel Flow with Transverse Square Bars on One Wall," *Journal of Fluid Mechanics*, Vol. 491, 2003, pp. 229–238.

[7]Jiménez, J., "Turbulent Flows over Rough Walls," *Annual Review of Fluid Mechanics*, Vol. 36, 2004, pp. 173–196.

[8]Miyake, Y., Tsujimoto, K., and Nagai, N., "Numerical Simulation of Channel Flow with a Rib–Roughened Wall," *Journal of Turbulence*, Vol. 3, 2002, p. 35.

[9]Ashrafian, A., and Anderson, H. I., "DNS of Turbulent Flow in a Rod–Roughened Channel," *Proceedings of the Turbulent and Shear Flow Phenomena 3*, edited by N. Kasagi, J. K. Eaton, R. Friedrich, J. A. C. Humphrey, M. A. Leschziner, and T. Miyauchi, Vol. 1, Sendai, Japan, 2003, pp. 117–123.

[10]Cui, J., Patel, V. C., and Lin, C. L., "Large–Eddy Simulation of Turbulent Flow in a Channel with Rib Roughness," *International Journal of Heat and Fluid Flow*, Vol. 24, No. 3, 2003, pp. 372–388.

[11]Hanjalic, K., and Launder, B. E., "Fully Developed Asymmetric Flow in Plane Channel," *Journal of Fluid Mechanics*, Vol. 51, 1972, pp. 301–335.

[12]Ikeda, T., and Durbin, P. A., "Direct Simulations of a Rough-Wall Channel Flow," Dept. of Mechanical Engineering, Stanford Univ., Rept. TF 81, Stanford, CA, 2002.

[13]Orlandi, P., *Fluid Flow Phenomena—A Numerical Toolkit*, Kluwer Academic, Dordrecht, The Netherlands, 2000.

[14]Fadlun, E. A., Verzicco, R., Orlandi, P., and Mohd-Yusof, J., "Combined Immersed Boundary Finite-Difference Methods for Three-Dimensional Complex Flow Simulations," *Journal of Computational Physics*, Vol. 161, No. 1, 2000, pp. 35–60.

[15]Iaccarino, G., and Verzicco, R., "Immersed Boundary Technique for Turbulent Flow Simulations," *Applied Mechanics Review*, Vol. 56, No. 3, 2003, pp. 331–347.

[16]Liu, C. K., Kline, S. J., and Johnston, J. P., "An Experimental Study of Turbulent Boundary Layers on Rough Walls," Dept. of Mechanical Engineering, Rept. MD–15, Stanford Univ., Stanford, CA, 1966.

[17]Leonardi, S., Orlandi, P., and Antonia, R. A., "A Method for Determining the Frictional Velocity in a Turbulent Channel Flow with Roughness on the Bottom Wall," *Experiments in Fluids*, Vol. 38, No. 6, 2005, pp. 796–800.

[18]Moser, R. D., Kim, J., and Mansour, N. N., "Direct Numerical Simulation of Turbulent Channel Flow up to $Re_\tau = 590$," *Physics of Fluids*, Vol. 11, No. 4, 1999, pp. 943–945.

[19]Bandyopadhyay, P. R., "Rough-Wall Turbulent Boundary Layers in the Transition Regime," *Journal of Fluid Mechanics*, Vol. 180, 1987, pp. 231–266.

[20]Bhaganagar, K., Kim, J., and Coleman, G., "Effect of Roughness on Wall-Bounded Turbulence," *Flow Turbulence and Combustion*, Vol. 72, Nos. 2–4, 2004, pp. 463–492.

[21]Orlandi P., Leonardi, S., Tuzi, R., and Antonia, A. R., "DNS of Turbulent Channel Flow with Wall Velocity Disturbances," *Physics of Fluids*, Vol. 15, No. 12, 2003, pp. 3497–3600.

[22]Smalley, R. J., Leonardi, S., Antonia, R., Djenidi, L., and Orlandi, P., "Reynolds Stress Anisotropy of Turbulent Rough Walls Layers," *Experiments in Fluids*, Vol. 33, No. 1, 2002, pp. 31–37.

[23]Krogstad, P. A., Anderson, H. I., Bakken, O. M., and Ashrafian, A., "An Experimental and Numerical Study of Channel Flow with Rough Walls," *Journal of Fluid Mechanics*, Vol. 530, 2005, pp. 327–352.

[24]Orlandi, P., and Leonardi, S., "DNS of Turbulent Channel Flows with Two- and Three-Dimensional Roughness," *Journal of Turbulence* (to be published).

L. Castillo
Associate Editor